SCIENTIFIC REPORTS

OPEN

Investigation on $LiBH_4$-CaH_2 composite and its potential for thermal energy storage

Received: 28 September 2016
Accepted: 28 December 2016
Published: 31 January 2017

Yang Li, Ping Li & Xuanhui Qu

The $LiBH_4$/CaH_2 composite are firstly studied as Concentrating Solar Power Thermal Storage Material. The $LiBH_4$/CaH_2 composite according to the stoichiometric ratio are synthesized by high-energy ball milling method. The kinetics, thermodynamics and cycling stability of $LiBH_4$/CaH_2 composite are investigated by XRD (X-ray diffraction), DSC (Differential scanning calorimeter) and TEM (Transmission electron microscope). The reaction enthalpy of $LiBH_4$/CaH_2 composite is almost 60 kJ/mol H_2 and equilibrium pressure is 0.482 MPa at 450 °C. The thermal storage density of $LiBH_4$/CaH_2 composite is 3504.6 kJ/kg. XRD results show that the main phase after dehydrogenation is LiH and CaB_6. The existence of $TiCl_3$ and NbF_5 can effectively enhance the cycling perfomance of $LiBH_4$/CaH_2 composite, with 6–7 wt% hydrogen capacity after 10 cycles. The high thermal storage density, high working temperature and low equilibrium pressure make $LiBH_4$/CaH_2 composite a potential thermal storage material.

Solar energy is the most plentiful renewable and clean alternative to fossil fuels[1]. International Energy Agency (IEA) points out that solar energy will make up 22 percent of the global electricity, and it is possible that solar photovoltaics (PV) and concentrating solar thermal (CST) power technology will play roughly equal, but complementary roles by 2050[2]. The CST power technology can store energy as heat that can be assessed on demand to generate electricity when PV technology is inefficient, such as at night or during rainy days.

As thermal storage (TS) material is the key element in the CST, improving the energy storage density and working temperature have great value on power generation efficiency and cutting back on the cost. There are three basic methods of thermal storage. Considering the condition of CST plants, sensible heat storage with molten salt is of low-efficiency and can be corrosive sometimes and latent heat storage using $NaNO_3$ is of high flammability and reactivity and is uncertain over its longevity. Thermochemical heat storage materials have quite high energy storage density, in which hydrides' exceed 1700–4000 kJ kg^{-1} (10~30 times more than molten salts' energy storage density and 4~10 times more than phase change materials' energy storage density)[3,4]. The characteristics of common and potential thermal storage materials are listed in Table 1.

Among all hydrides, complex hydrides such as $LiBH_4$, $NaAlH_4$ and $NaBH_4$ possess a quite high forming enthalpy due to the transition to an ionic or covalent compound of metals upon hydrogen absorption[9] It seems that complex hydrides are promising thermal storage materials in CST plants.

In fact, $LiBH_4$ is mostly researched as a hydrogen storage material due to the second highest hydrogen content (18.4 wt.%) of all alanates and boranates[10–13]. The thermal hydrogen desorption of pure $LiBH_4$ starts at ~320 °C and proceeds mainly in the temperature region 400–600 °C, which is in accordance with the working temperature of thermal storage material in CST plant.

$$LiBH_4 \rightarrow LiH + B + 3/2H_2,\ \Delta_r H = 74\ kJ\ mol^{-1}H_2 \quad (1)$$

However, the sluggish kinetics and poor reversibility of $LiBH_4$ are the problems that limit its use in hydrogen storage[11–13]. The destabilization was proposed to change the reaction process by adding a reactive additive[14]. Thus, many new systems have been proposed based on DFT calculation of reaction enthalpies in multi-component systems[15,16]. Among all systems, $LiBH_4$-CaH_2 is one of promising composites that are suitable for thermal storage due to its onset temperature. And this reaction can produce around 11.7 wt% hydrogen. But Yang reported that

State Key Laboratory for Advanced Metals and Materials, Institute for Advanced Materials and Technology, University of Science and Technology Beijing, Beijing 100083, China. Correspondence and requests for materials should be addressed to P.L. (email: ustbliping@126.com)

Material	Sensible		Latent		Thermochemical	
	Rock	Concrete	Paraffin wax	$NaNO_3$	$CaCl_2{\cdot}H_2O$	MgH_2
Specific heat capacity (kJ kg^{-1})	0.9	1.13	—	—	3.06	—
Latent heat of fusion (kJ kg^{-1})	—	—	174.4	172	—	—
Reaction enthalpy (kJ kg^{-1})	—	—	—	—	433.6	2860

Table 1. Energy stored per mass of different storage materials[5–8].

$LiBH_4$-CaH_2 composite is irreversible under the condition tested (350 °C, 150 bar)[17]. The sluggish kinetics in $LiBH_4$-CaH_2 composite is another problem that need to be solved[18].

$$6LiBH_4 + CaH_2 \rightarrow 6LiH + CaB_6 + 10H_2 \quad (2)$$

Additives, such as $TiCl_3$[19–23], V_2O_5[19], TiF_3[19,20], TiO_2[19,20], $LiNH_2$[19], NbF_5[24,25], $NbCl_5$[24] were investigated their effects on the kinetics and cycling performance of $LiBH_4$-CaH_2 composite. Results show that $TiCl_3$ additive is very effective in lowering activation energy of dehydrogenation and enhancing reversibility (about 9 wt% hydrogen reversibly)[19–23]. Besides, Lim reported that $LiBH_4$-CaH_2 composite with NbF_5 maintains a reversible hydrogen storage capacity of about 6 wt% at 450 °C[25].

But the enthalpies of pure $LiBH_4$-CaH_2 composite and $LiBH_4$-CaH_2 composite with additives have not been reported exactly. Pinkerton[21] reported the estimated enthalpy of reaction 2 at 400 °C is $\Delta H = 59.2$ kJ/mol H_2. Lim[24] reported that the reaction enthalpy of $LiBH_4$-CaH_2-0.2NbF_5 composite is estimated to be 56.5 kJ/mol H_2 at 305 °C. But according to HSC thermochemical database[21], the enthalpy is 66.2 kJ/mol H_2 at room temperature.

In this research, the enthalpy ΔH and equilibrium pressure of desorption according to reaction 2 are determined by PCT (pressure, concentration, and temperature) measurements. Only $LiBH_4$-CaH_2 without catalysts was measured due to the fact that influence the thermodynamics of the mixture as Ti-doped $NaAlH_4$[12]. The additives such as $TiCl_3$ and NbF_5 are investigated their effect on kinetics and cycling performance of $LiBH_4$-CaH_2 composite.

Experimental Details

$LiBH_4$ (≥95% pure), purchased from Acros Organics, CaH_2 (≥98% pure) and NbF_5 (≥ 99% pure), purchased from Alfa Aesar, and $TiCl_3$ (≥95% pure), synthesized by the reaction of titanium tetrachloride with metallic titanium in molten $CaCl_2$ and the enrichment process with HCl gas[26], were utilized directly without any further purification. The mole ratio of $LiBH_4$-CaH_2 composite according to reaction 2 is 6:1. The pure $LiBH_4$-CaH_2 composite and $LiBH_4$-CaH_2 composite doped with different additives (1 mol% $TiCl_3$, and 5 wt% NbF_5) was ball-milled under argon atmosphere by using a QM-2B high energy mill (Nanjing NanDa Instrument Plant) at a rotating speed of 1200 rpm for 1 h. Two kinds of stainless steel balls with 4 mm and 8 mm diameters were added with a ball-to powder weight ratio of 12.5:1. Typically, 4 g mixture was sealed in the stainless steel vessel within a high purity argon atmosphere during milling. To avoid excess heating of the stainless steel vessel, there were 10 min intervals between each 5 min milling process.

The isothermal desorption was measured by using the Sieverts-type pressure-composition-temperature (P-C-T) apparatus (General Research Institute for Nonferrous Metals, China). The maximum pressure, maximum vacuum degree and maximum temperature of this apparatus is 10 MPa, 10^{-1} Pa and 800 °C, respectively. Typically, 60–100 mg sample was loaded into the vessel, and then heated up to 450 °C under 0.1 MPa hydrogen atmosphere. Following the dehydrogenation, the samples were subjected to rehydrogenation studies at 450 °C under 8 MPa hydrogen pressure for 16 h. It should be noted that the additional content was not taken into consideration when calculating the released hydrogen. The PCI (Pressure-composition isotherms) curves were measured at 405 °C, 420 °C, 435 °C, 450 °C and 465 °C, respectively.

The phase structure of the samples after milling and dehydrogenation was examined by an MXP21VAHF X-ray Diffractometer (XRD with Cu Kα radiation, 40 kV, 300 mA), with the 2θ angle ranged from 10° to 90° with a scanning rate of 10° min^{-1}. X-ray photoelectron spectroscopy (XPS) was performed with the PHI-5300 spectrometer. The morphology and phase constitution of all samples after ball milling and desorption were observed by and transmission electron microscopy (Tecnai G2 F30 S-TWIN, FEI, USA). Simultaneous differential scanning calorimetry (DSC) and Thermogravimetric Analysis (TGA) experiments were conducted under 50 mL min^{-1} argon flow in a NETZSCH STA 449F3 Jupiter instrument between 50 °C and 500 °C with a heating rate of 5 °C min^{-1}. The samples were transferred to Al_2O_3 crucibles under argon atmosphere for the DSC-TGA measurements.

All samples handling was performed under strictly inert conditions (≥99.99% Ar atmosphere) in the glove box (Mikrouna, Super-750) equipped with oxygen/humidity sensors and recirculation system to avoid oxidation and moisture. Oxygen and H_2O levels were kept below 0.1 ppm.

Results and Discussion

XPS characterization. The XPS results of three $LiBH_4$-CaH_2 composites after milling are presented in Fig. 1(a–c), which confirms the existence of element Li, B and Ca in both composites. Element Nb, F and Cl are identified in the catalyst-doped composite, while Ti are not discovered due to the low amount addition. The XRD results are presented in Fig. S1. There are only two obvious peaks in both composites, which are characterized as CaH_2. It can be inferred that the structure of $LiBH_4$ after milling becomes amorphous. No peaks of $LiBH_4$, $TiCl_3$ or NbF_5 are detected. The XPS narrow spectra of ball-milled $LiBH_4$-CaH_2 composite are showed in Fig. 1(d). The

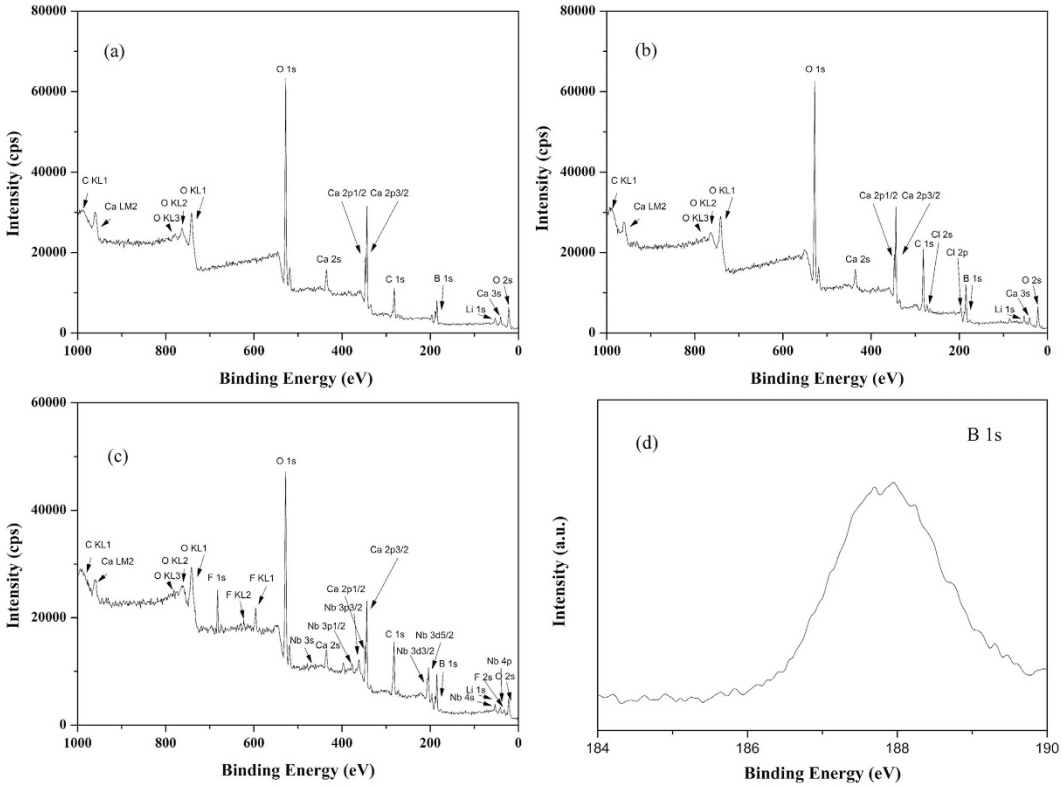

Figure 1. XPS scan spectra of three $LiBH_4$-CaH_2 composites after ball milling: (**a**) pure composite (**b**) 1 mol% $TiCl_3$ addition (**c**) 5 wt% NbF_5 addition (**d**) B 1 s in pure composite.

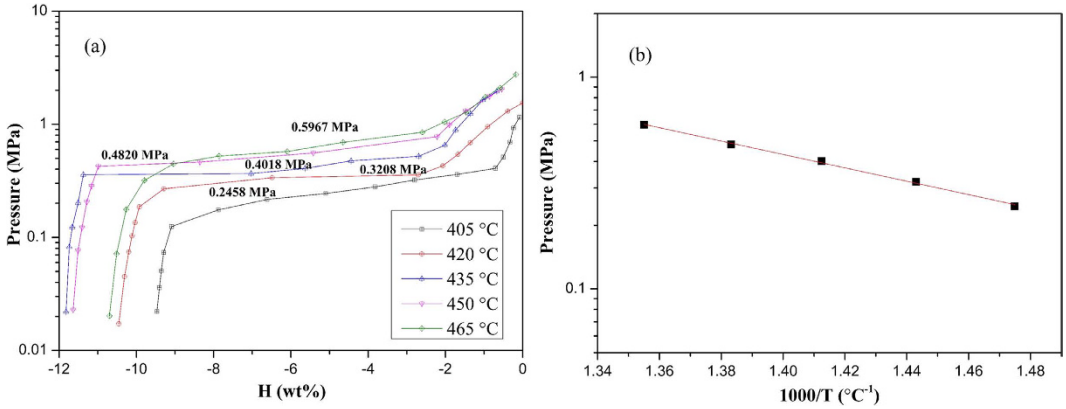

Figure 2. (**a**) Dehydrogenation PCI curves, (**b**) Dehydrogenation van't hoff curves of pure $LiBH_4$-CaH_2 composite.

photo-emission spectrum of B 1 s at 187.8 eV corresponds to $LiBH_4$, while the existence of LiCl and NbF_5 are also convinced in Fig. S2. XPS results testify that $LiBH_4$ and $TiCl_3$ react during ball milling[22].

Investigation on energy storage density. The energy storage density is the most significant factor when evaluating a material is suitable for TS. The energy storage density to weight is related with the reaction enthalpy and molar mass. For dehydrogenation reaction of hydrides, the Van't hoff equation and DSC integration can be used to calculate the reaction enthalpy. Besides high energy storage density, low equilibrium pressure and high working temperature are also two important factors in selecting hydrides for TS.

PCI curves and Van't Hoff Calculation. The dehydrogenation PCI curves of pure $LiBH_4$-CaH_2 composite are shown in Fig. 2(a). Due to the sluggish kinetics, the pressure value in each platform can only be read after 4-hours waiting. Even so, the platform inclination is quite a lot, especially in low temperature condition. Considering the platform is a slope to some extent, the equilibrium pressures from 405 °C to 465 °C are calculated

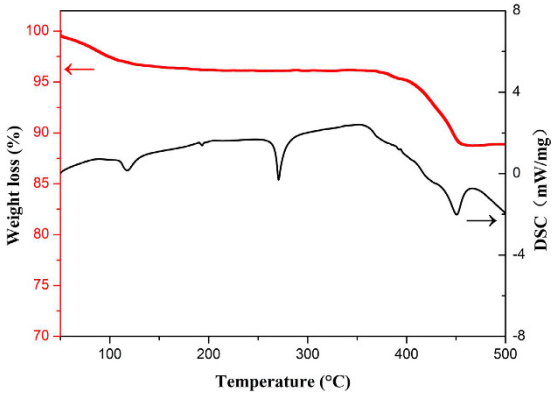

Figure 3. DSC and TGA curves of pure $LiBH_4$-CaH_2 composite.

	H_2 content (wt%)	Enthalpy (kJ mol^{-1} H_2)	TS density (kJ kg^{-1})	Equilibrium temperature at 1 bar [°C]
MgH_2	7.6	74.4	2860	280
$NaMgH_3$*	4.0	86	1700	380
Mg_2FeH_6	5.5	77.4	2106.5	320
Mg_2NiH_6	3.6	62	1116	250
CaH_2	4.8	186.2	4422.8	950
$Ce_2Mg_{17}H_x$	5.0	75.5	1926.3	310
$LiBH_4$-CaH_2	11.7	60.706	3511.45	350
$LiBH_4$-CaH_2-1 mol% $TiCl_3$	11.6	59.354	3316.64	—
$LiBH_4$-CaH_2-5 wt% NbF_5	10.4	60.011	3307.71	—

Table 2. TS properties of three $LiBH_4$-CaH_2 composites and other potential TS composites[4,6,8,9,30]. *Calculated for the reaction $NaMgH_3 \rightleftarrows NaH + Mg + H_2$.

as the mean of pressure values in the platform. The equilibrium pressures of pure $LiBH_4$-CaH_2 composite from 405 °C to 465 °C are 0.2458 MPa, 0.3208 MPa, 0.4018 MPa, 0.4820 MPa and 0.5967 MPa, respectively. They are lower than the equilibrium pressures of reported thermal storage metal hydrides, such as MgH_2, Mg_2FeH_6 and $Ce_2Mg_{17}H_x$[4,6,8]. What's more, the low equilibrium pressure makes $LiBH_4$-CaH_2 composite possible to be operated at higher temperature. The higher working temperature can increase overall solar to electricity conversion efficiency and reduce the cost in CST plants[27]. The dehydrogenation capacity of pure $LiBH_4$-CaH_2 composite is mostly ranging from 10.5 wt% to 11.6 wt%, which is close to their theoretical value. The sluggish kinetics resulting from the relatively low temperature (405 °C) may account for the lower capacity (9.5 wt%). Only $LiBH_4$-CaH_2 without catalysts was measured due to the fact that influence the thermodynamics of the mixture as Ti-doped $NaAlH_4$[12]. Liu[22] reported that LiCl forms during ball milling of $6LiBH_4/CaH_2/xTiCl_3$. LiF and CaF_2 are observed after the ball milling reaction of NbF_5 and $LiBH_4$ or CaH_2[24]. Thermodynamics of pure $LiBH_4$-CaH_2 composite might have changed due to the formation of LiCl or LiF and CaF_2.

A plot of ln P against 1000/T in Fig. 2(b) results in a nearly straight line. Calculation of $\Delta H = R \cdot (\ln P_2 - \ln P_1)/(1/T_2 - 1/T_1)$ from ln P and 1/T values at 405 °C and 465 °C provides a ΔH of 60.555 kJ mol^{-1} H_2. According to the reaction 2, a thermal storage density value of 3504.6 kJ kg^{-1} is calculated. It shows a superior capacity to sensible and latent thermal storage materials, even to thermochemical thermal storage materials shown in Table 1.

DSC Calculation. The DSC and TGA curves of pure $LiBH_4$-CaH_2 composite are shown in Fig. 3. There are mainly three endothermic peaks during the heating process. The endothermic effect at 108–112 °C is reversible and corresponds to polymorphic transformation of $LiBH_4$. The second peak at 268–286 °C corresponds to the fusion of $LiBH_4$. The third peak corresponds to the dehydrogenation behavior of $LiBH_4$. The onset temperature is 392 °C and the peak temperature is 446 °C. According to TGA results, dehydrogenation reaction ends at 497 °C. The integration of DSC on temperature from 392 °C to 497 °C is calculated as enthalpy of reaction 2, with a value of 60.706 kJ mol^{-1} H_2.

The DSC and TGA curves of $LiBH_4$-CaH_2 composites with $TiCl_3$ and NbF_5 addition are shown in Fig. S3. There are both three endothermic peaks in these two composites. NbF_5 addition shows a more remarkable influence on the decrease of onset temperature than $TiCl_3$. The onset temperature, dehydrogenation reaction enthalpy and thermal storage density of three composites and other potential TS system are shown in Table 2. The $TiCl_3$ doped composite and NbF_5 doped composite shows similar reaction enthalpy as the pure $LiBH_4$-CaH_2 composite. It can be speculated that catalyst additions in $LiBH_4$-CaH_2 composite do not have a remarkable influence on the dehydrogenation reaction enthalpy. The TS density of pure composite is the highest (3511.45 kJ kg^{-1}), while $TiCl_3$ and NbF_5 doped composites possess nearly 3300 kJ kg^{-1} TS density, with a little reduction. The DSC calculation

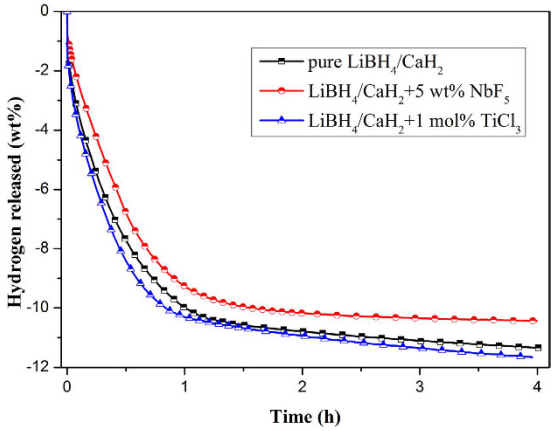

Figure 4. Isothermal dehydrogenation curves of different $LiBH_4$-CaH_2 composites under 450 °C and H_2 atmosphere (0.1 MPa).

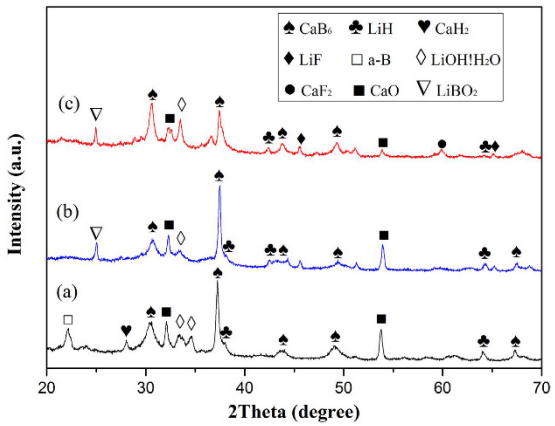

Figure 5. XRD patern of three $LiBH_4$-CaH_2 composites after desorption: (**a**) pure composite (**b**) 1 mol% $TiCl_3$ addition (**c**) 5 wt% NbF_5 addition.

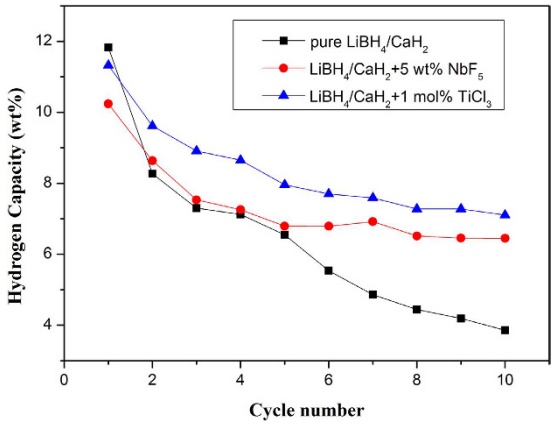

Figure 6. Cycling curves of three $LiBH_4$-CaH_2 composites.

results are in accordance with the Van't hoff calculation results. Comparing with actual TS density of MgH_2 (2147 kJ kg^{-1})[28,29], $LiBH_4$-CaH_2 composites shows a clear superiority.

Investigation on kinetics. The Fig. 4 shows the desorption behavior of three $LiBH_4$-CaH_2 composites. The addition of $TiCl_3$ significantly improves the dehydrogenation kinetics of $LiBH_4$-CaH_2 composite, while NbF_5 influence it in an opposite way. Both composites can release 9–10 wt% hydrogen in an hour. After 4 hours, the

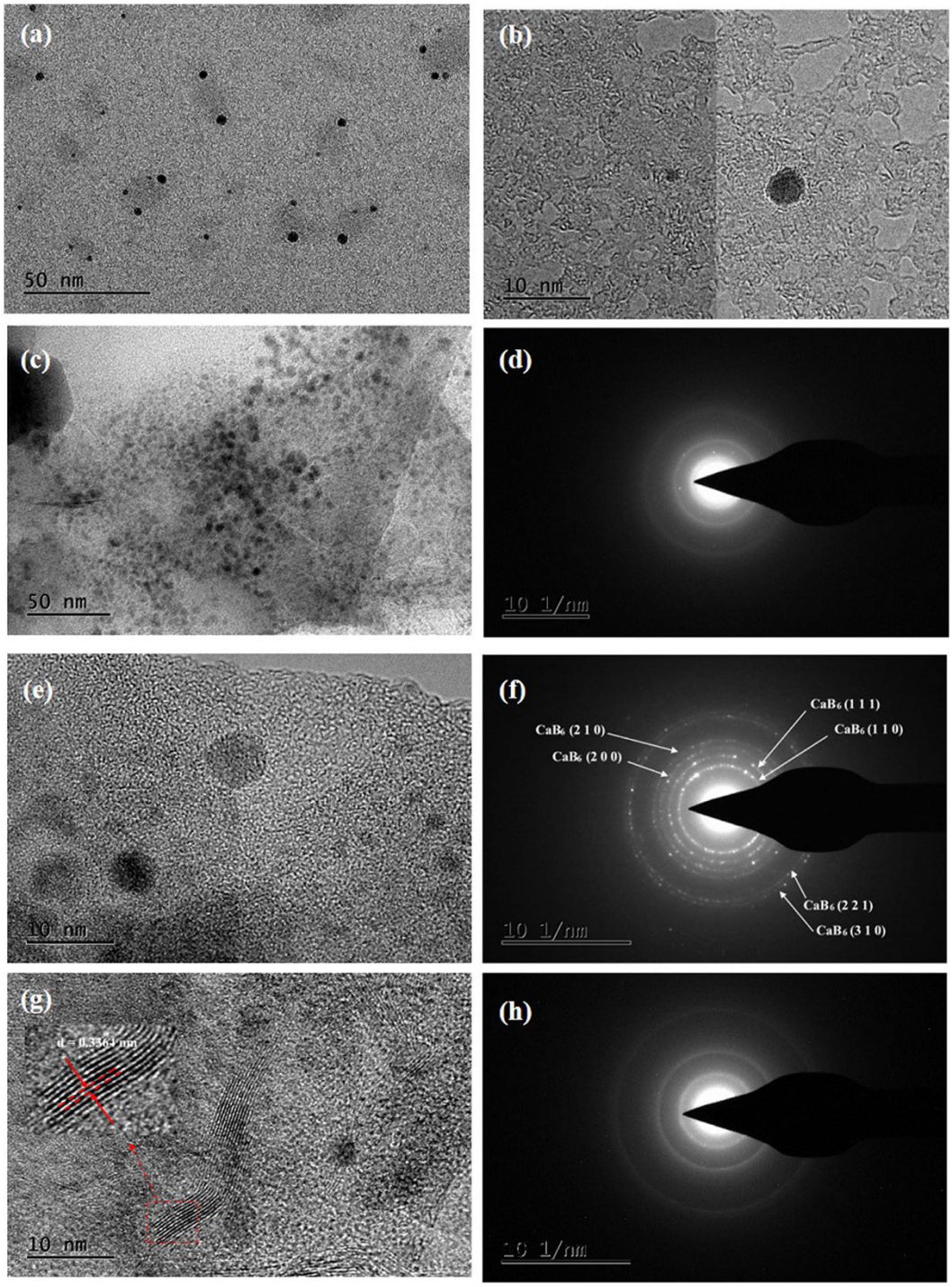

Figure 7. TEM and SAED images: (**a**–**d**) pure $LiBH_4$-CaH_2 composite after 10 cycles; (**e**,**f**) $TiCl_3$ doped composite after 10 cycles; (**g**,**h**) of NbF_5 doped composite after 10 cycles.

pure composite and $TiCl_3$ doped composite shows a nearly theoretical hydrogen capacity (11.7 wt%), while NbF_5 doped composite only desorbs around 10 wt% hydrogen. $TiCl_3$ shows a remarkable impact on improving the desorption kinetics and maintaining the hydrogen capacity. Liu[22] reported that LiCl formed through replacement reaction between $LiBH_4$ and $TiCl_3$ during ball milling can be incorporated into $LiBH_4$ to form solid solution $LiBH_4$·LiCl. It favorably changes viscosity, preserving the nano-sized phase arrangement formed after milling, leading to fast kinetics.

The XRD results of three $LiBH_4$-CaH_2 composites after dehydrogenation are shown in Fig. 5. The main phase of both composites is LiH and CaB_6, which is in accordance with reaction 2. The existence of phase CaO, LiOH!H_2O and $LiBO_2$ is due to the oxidation during the experiments. The remaining CaH_2 and B are identified in the pure composite after dehydrogenation. B is the product of $LiBH_4$ after dehydrogenation (shown in reaction 1),

which also explains why a little CaH_2 remains. The LiF and CaF_2 phase are detected in the NbF_5 doped composite, while no peaks of chlorides are identified in the $TiCl_3$ doped composite.

Investigation on reversibility and cycling stability performance. A test over 10 cycles was performed under very severe cycling conditions (desorption: 450 °C, 0.1 Mpa,4 h; absorption: 450 °C, 8 MPa, 16 h). The results are shown in Fig. 6. The initial hydrogen capacity of the pure composite and $TiCl_3$ doped composite shows a nearly theoretical hydrogen capacity (11.7 wt%), while NbF_5 doped composite only desorbs around 10 wt% hydrogen. The hydrogen capacity of both composites declines during cycling. It is worth mentioning that $TiCl_3$ doped composite can reversibly store 9 wt% hydrogen during first three cycles. After 10 cycles, the remaining hydrogen capacity of pure composite, NbF_5 doped composite and $TiCl_3$ doped composite is 3.8 wt%, 6.4 wt% and 7.1 wt%, respectively. $TiCl_3$ and NbF_5 seems effectively raise the cycling stability performance of $LiBH_4$-CaH_2 composite.

The TEM images of pure $LiBH_4$-CaH_2 composite after 10 cycles are shown in Fig. 7(a–d). The main phases are small particles with a diameter of 3–6 nm, separately scattering. Particle aggregation shown in Fig. 7(c), which may result from the sintering, is also found. The diffraction ring in Fig. 7(d) is very obvious, indicating that amorphous structure is formed. The particle aggregation and amorphous structure of products accounts for the dramatic loss of hydrogen capacity of pure $LiBH_4$-CaH_2 composite during cycling. TEM images of $TiCl_3$ doped composite and NbF_5 doped composite after 10 cycles are shown in Fig. 7(e,f,g and h). The small particles with a diameter of 3–6 nm are both observed. However, the results of electron diffraction indicate that the $TiCl_3$ doped composite after 10 cycles is crystal structure, while NbF_5 doped composite after 10 cycles is amorphous structure. By analyzing the diffraction ring diameter, the crystal structure is assumed to be CaB_6. The amorphous structure of B is not good for the reverse reaction to produce $LiBH_4$, while the crystal structure of CaB_6 is in favor of the reverse reaction[29,31,32]. This explains why $TiCl_3$ plays a more effective role in raising the cycling stability performance of $LiBH_4$-CaH_2 composite than NbF_5. Moreover, it is noteworthy that a graphene-like lamellar structure are found in NbF_5 doped composite after 10 cycles. The value of interlamellar spacing (d) is 0.3364 nm, which is corresponding to NbF_5. But the lamellar structure of NbF_5 is never reported. Thus, the d value of NbB_2 is 0.3321 nm, which is close to the 0.3364 nm. Minella reported that NbB_2 nanoparticles was observed after milling or upon sorption reactions of Nb-based $Ca(BH_4)_2$ doped composites[33]. It is reasonable to be assume that a small amount of NbB_2 can also be formed in Nb-based $LiBH_4$-CaH_2 doped composites. It needs more research work to identify this graphene-like lamellar structure in NbF_5 doped composite.

Conclusion

The reaction enthalpy of $LiBH_4/CaH_2$ composite is almost 60 kJ/mol H_2 and equilibrium pressure is 0.482 MPa at 450 °C. The thermal storage density of $LiBH_4/CaH_2$ composite is 3504.6 kJ/kg. XRD results show that the main phase after dehydrogenation is LiH and CaB_6. The exsience of $TiCl_3$ and NbF_5 can effectively enhance the cycling perfomance of $LiBH_4/CaH_2$ composite, with 6–7 wt% hydrogen capacity after 10 cycles. The high thermal sotrage density, high working temperature and low equilibrium pressure make $LiBH_4/CaH_2$ composite a potential thermal storage material.

Although the high price of starting materials, such as $LiBH_4$, will limit its usage, the $LiBH_4/CaH_2$ composite could serve as the additives for Magnesium-based alloys in TS. The research will be continued on the pair study of $LiBH_4/CaH_2$ composite with another metal hydride working at lower temperature.

References

1. Kalogirou, S. A. *Solar energy engineering: processes and systems*. (Academic Press, 2013).
2. Birol, F. World energy outlook 2010. *International Energy Agency 1* (2010).
3. Liu, C., Li, F., Ma, L. P. & Cheng, H. M. Advanced materials for energy storage. *Advanced materials* **22** (2010).
4. Felderhoff, M., Urbanczyk, R. & Peil, S. Thermochemical heat storage for high temperature applications–a review. *Green* **3,** 113–123 (2013).
5. Agyenim, F., Hewitt, N., Eames, P. & Smyth, M. A review of materials, heat transfer and phase change problem formulation for latent heat thermal energy storage systems (LHTESS). *Renewable and sustainable energy reviews* **14,** 615–628 (2010).
6. Qu, X., Li, Y., Li, P., Wan, Q. & Zhai, F. The development of metal hydrides using as concentrating solar thermal storage materials. *Frontiers of Materials Science* **9,** 317–331 (2015).
7. Mueller, W. M., Blackledge, J. P. & Libowitz, G. G. *Metal hydrides*. (Elsevier, 2013).
8. Li, Y., Li, P., Wan, Q., Zhou, C. & Qu, X. A study of metal hydride as novel thermal energy storage material by using rapid solidification. *Journal of Alloys and Compounds* **689,** 641–647 (2016).
9. Züttel, A., Borgschulte, A. & Schlapbach, L. *Hydrogen as a future energy carrier*. (John Wiley & Sons, 2011).
10. Züttel, A. *et al.* $LiBH_4$ a new hydrogen storage material. *Journal of Power Sources* **118,** 1–7 (2003).
11. Züttel, A. *et al.* Hydrogen storage properties of $LiBH_4$. *Journal of Alloys and Compounds* **356,** 515–520 (2003).
12. Mauron, P. *et al.* Stability and reversibility of $LiBH_4$. *The Journal of Physical Chemistry B* **112,** 906–910 (2008).
13. Mosegaard, L. *et al.* Reactivity of $LiBH_4$: *in situ* synchrotron radiation powder X-ray diffraction study. *The Journal of Physical Chemistry C* **112,** 1299–1303 (2008).
14. Vajo, J. J., Salguero, T. T., Gross, A. F., Skeith, S. L. & Olson, G. L. Thermodynamic destabilization and reaction kinetics in light metal hydride systems. *Journal of Alloys and Compounds* **446,** 409–414 (2007).
15. Alapati, S. V., Johnson, J. K. & Sholl, D. S. Identification of destabilized metal hydrides for hydrogen storage using first principles calculations. *The Journal of Physical Chemistry B* **110,** 8769–8776 (2006).
16. Alapati, S. V., Johnson, J. K. & Sholl, D. S. Predicting reaction equilibria for destabilized metal hydride decomposition reactions for reversible hydrogen storage. *The Journal of Physical Chemistry C* **111,** 1584–1591 (2007).
17. Yang, J., Sudik, A. & Wolverton, C. Destabilizing libh4 with a metal (M = Mg, Al, Ti, V, Cr, or Sc) or metal hydride (MH_2 = MgH_2, TiH_2, or CaH_2). *The Journal of Physical Chemistry C* **111,** 19134–19140 (2007).
18. Ibikunle, A., Sabitu, S. & Goudy, A. Kinetics and modeling studies of the $CaH_2/LiBH_4$, $MgH_2/LiBH_4$, $Ca(BH_4)_2$ and $Mg(BH_4)_2$ systems. *Journal of Alloys and Compounds* **556,** 45–50 (2013).
19. Ibikunle, A., Goudy, A. & Yang, H. Hydrogen storage in a $CaH_2/LiBH_4$ destabilized metal hydride system. *Journal of Alloys and Compounds* **475,** 110–115 (2009).

20. Yang, H., Ibikunle, A. & Goudy, A. J. Effects of Ti-Based Additives on the Hydrogen Storage Properties of a/Destabilized System. *Advances in Materials Science and Engineering 2010* (2010).
21. Pinkerton, F. & Meyer, M. Reversible hydrogen storage in the lithium borohydride—calcium hydride coupled system. *Journal of Alloys and Compounds* **464,** 1–4 (2008).
22. Liu, D., Yang, J., Ni, J. & Drews, A. Studies of the effects of $TiCl_3$ in $LiBH_4/CaH_2/TiCl_3$ reversible hydrogen storage system. *Journal of Alloys and Compounds* **514,** 103–108 (2012).
23. Jin, S. A., Lee, Y. S., Shim, J. H. & Cho, Y. W. Reversible hydrogen storage in $LiBH_4-MH_2$ (M = Ce, Ca) composites. *The Journal of Physical Chemistry C* **112,** 9520–9524 (2008).
24. Lim, J. H., Shim, J. H., Lee, Y. S., Cho, Y. W. & Lee, J. Dehydrogenation behavior of $LiBH_4/CaH_2$ composite with NbF_5. *Scripta Materialia* **59,** 1251–1254 (2008).
25. Lim, J.-H. *et al.* Rehydrogenation and cycle studies of $LiBH_4$–CaH_2 composite. *International journal of hydrogen energy* **35,** 6578–6582 (2010).
26. Song, J., Wang, Q., Kang, M. & Jiao, S. Novel Synthesis of High Pure Titanium Trichloride in Molten $CaCl_2$. *Int. J. Electrochem. Sci* **10,** 919–930 (2015).
27. Sheppard, D. *et al.* Hydriding characteristics of $NaMgH_2F$ with preliminary technical and cost evaluation of magnesium-based metal hydride materials for concentrating solar power thermal storage. *RSC Advances* **4,** 26552–26562 (2014).
28. Reiser, A., Bogdanović, B. & Schlichte, K. The application of Mg-based metal-hydrides as heat energy storage systems. *International Journal of Hydrogen Energy* **25,** 425–430 (2000).
29. Yan, Y. *et al.* Controlling the dehydrogenation reaction toward reversibility of $LiBH_4$–$Ca(BH_4)_2$ eutectic system. *The Journal of Physical Chemistry C* **117,** 8878–8886 (2013).
30. Harries, D. N., Paskevicius, M., Sheppard, D. A., Price, T. E. C. & Buckley, C. E. Concentrating solar thermal heat storage using metal hydrides. *Proceedings of the IEEE* **100,** 539–549 (2012).
31. Javadian, P., Sheppard, D. A., Buckley, C. E. & Jensen, T. R. Hydrogen storage properties of nanoconfined $LiBH_4$–$Ca(BH_4)_2$. *Nano Energy* **11,** 96–103 (2015).
32. Gu, J. *et al.* Improved hydrogen storage properties of combined $Ca(BH_4)_2$ and $LiBH_4$ system motivated by addition of $LaMg_3$ assisted with ball milling in H_2. *International Journal of Hydrogen Energy* **40,** 12325–12335 (2015).
33. Bonatto Minella, C. *et al.* Chemical state, distribution, and role of Ti-and Nb-based additives on the $Ca(BH_4)_2$ system. *The Journal of Physical Chemistry C* **117,** 4394–4403 (2013).

Acknowledgements

This study was financially supported by the National Natural Science Foundation of China (Grant No. 51471054) and Natural Science Foundation of Beijing Municipality (2152019).

Author Contributions

Ping Li and Yang Li designed and conceived research. Yang Li wrote the manuscript. All authors read and approved the final version of the manuscript.

Additional Information

Supplementary information accompanies this paper at http://www.nature.com/srep

Competing financial interests: The authors declare no competing financial interests.

How to cite this article: Li, Y. *et al.* Investigation on $LiBH_4$-CaH_2 composite and its potential for thermal energy storage. *Sci. Rep.* **7**, 41754; doi: 10.1038/srep41754 (2017).

Publisher's note: Springer Nature remains neutral with regard to jurisdictional claims in published maps and institutional affiliations.